COMMUNICATION

Check for updates

Rapid, facile synthesis of Fe^{2+}-MOFs in water at ambient conditions

Ilia Kochetygov [ID] * and Davide Ferri [ID] *

The MOF-74 series of materials is known for its promising applications in gas capture and catalysis owing to the high density of open metal sites. Nevertheless, only a few materials are commonly accessible synthetically due to the resource-intensive solvothermal protocols. In this work, an aqueous and facile synthetic process was developed and demonstrated for two Fe-based members of the series. Using a combination of *in situ* infrared spectroscopy (IR) and high-energy X-ray diffraction (XRD), we shed light on the synthesis parameters and find optimal synthesis conditions for both materials. The synthetic utility of the method has been confirmed by isolating the same materials in the laboratory and by demonstrating the Fe^{2+} oxidation state using NO as a probe molecule.

Metal–organic frameworks (MOFs) are a versatile class of crystalline and porous materials formed by the coordination of metal ions or clusters with organic linkers. They exhibit unique structural and functional properties, such as ultrahigh porosity, tunable chemical environments, and responsiveness to external stimuli.[1] Their modularity allows one to tailor MOFs for specific applications, such as gas storage, separations, catalysis, drug delivery, environmental remediation, and more.[2]

Despite their versatility, the MOF synthesis remains critical in realizing their promising properties on an applied scale.[3] Parameters such as solvent type, temperature, reaction time, and metal-to-ligand ratios strongly influence the crystal size, porosity, stability, and eventually applicability of the resulting materials.[4] Therefore, the development of innovative, efficient, and environmentally friendly synthesis methods remains an essential area of applied MOF research.[5]

Traditional MOF synthesis methods rely on organic solvents such as dimethylformamide (DMF) that serve as reaction media to dissolve precursors and facilitate crystal growth.[6] However, such solvents present significant environmental and practical hazards: they are toxic, expensive, and require extensive post-synthetic purification steps to remove their residues, adding complexity and cost to the process.[7] High temperatures and long reaction times used in conventional syntheses further complicate large-scale MOF implementation.[8] These challenges necessitate the exploration of alternative synthesis methods that are more environmentally benign, cost-effective, and scalable.[9]

Water as a solvent offers several advantages over traditional organic solvents in MOF synthesis as it is abundant, inexpensive, and non-toxic.[10] The use of water avoids the need for rigorous solvent recovery or disposal, simplifying the production process and reducing its environmental footprint.[11] Beyond these benefits, water also plays an active role during MOF formation. Its high polarity and hydrogen-bonding capacity facilitate ligand deprotonation and metal hydrolysis, promoting the generation of metal-oxo and hydroxo clusters acting as secondary building units for framework nucleation.[12] Despite these advantages, the main challenge with the aqueous MOF synthesis is its specificity to only certain metal ions and ligands, mainly dictated by the limited solubility of ligands.[13] While this can be alleviated, for example, by using sodium hydroxide to deprotonate the ligands and solubilize the resulting carboxylate anions in water, this treatment also accelerates the reaction kinetics due to the higher reactivity of the anionic species.[14] Several examples show that these approaches succeed in producing high-quality MOF materials,[15] while in other cases, rapid coordination between the ligands and metal ions results in uncontrolled nucleation and growth processes, producing poorly crystalline or amorphous materials.[16]

MOF-74 represents a prominent class of materials combining high porosity, high density of open metal sites, and robust structural stability owing to the rigid honeycomb-like structure.[17] A high density of open metal sites, which serve as strong adsorption sites for selected molecules, renders these materials unparalleled in gas separation, *e.g.* CO$_2$ capture,[18] and separation of hydrocarbons[19] and O$_2$/N$_2$.[20] Adsorption affinity and chemical properties can be tuned using Mg, Ca, Sr, Ba, Mn, Fe, Co, Ni, Zn, and Cd metal ions as building blocks, offering a wide choice of frameworks for specific applications.[21] However, so far, only the Zn, Co, Mg, and Ni members of the series were successfully produced using the

Paul Scherrer Institute, PSI Center for Energy and Environmental Sciences, Forschungsstrasse 111, CH-5232 Villigen PSI, Switzerland.
E-mail: ilia.kochetygov@psi.ch, davide.ferri@psi.ch

aqueous synthesis,[22] limiting the choice when scalability and green synthesis nature are important. Among these variants, Fe-based MOFs are particularly attractive because iron combines redox flexibility, high natural abundance, and environmental benignity.[23] The Fe^{2+}/Fe^{3+} couple imparts tunable electronic and catalytic properties relevant to oxidation catalysis,[24] gas sorption,[20] and electrochemical transformations.[25] Fe-based frameworks also align with sustainable chemistry goals by replacing expensive or toxic metals commonly used in MOFs.[26]

Despite these advantages, aqueous synthesis of Fe^{2+} MOFs remains difficult due to the rapid oxidation of Fe^{2+} in water under air. Nevertheless, a few Fe^{2+} frameworks of Hofmann and Prussian Blue type have been obtained directly from aqueous solutions when oxygen exclusion, controlled pH, and stabilizing ligands are employed.[23,27] To date, however, no study has achieved a fully aqueous synthesis of Fe-MOF-74 or its analogues. Prior Fe-MOF-74 preparations have required solvothermal or mixed organic-aqueous systems using coordinating solvents such as DMF or MeOH.[19a,28] The absence of a direct water-based route limits both the sustainability and mechanistic understanding of Fe^{2+} coordination chemistry in this archetypal framework.

Here, we develop the facile aqueous synthesis of Fe-MOF-74 using the 2,5-dioxido-1,4-benzenedicarboxylate ligand (p-dobdc^{4-}, Fig. 1a) and its *meta*-isomer 4,6-dioxido-1,3-benzenedicarboxylate (m-dobdc^{4-}, Fig. 1b) with Fe in oxidation state 2+. Optimal synthesis conditions of Fe$_2$(p-dobdc) and Fe$_2$(m-dobdc) were identified using *in situ* attenuated total reflection infrared spectroscopy (ATR-IR) and high-energy time-resolved X-ray diffraction (XRD) that allowed their preparative production on a larger scale.

When Fe(ClO$_4$)$_2$ was used as a starting material in the *in situ* cell and the reaction was carried out under air, a clear spectrum similar to that of Zn$_2$(p-dobdc)[29] appeared in the sequence of *in situ* ATR-IR spectra after only *ca.* 12 s (Fig. 1c and Fig. S1), indicating a prompt formation of the MOF material within seconds. However, the intensity of the main features of this spectrum decreased over time, and a new spectrum appeared with broader and shifted peaks (Fig. 1c). These important spectral changes suggest that under these synthesis conditions, decomposition/amorphization of the Fe-MOF occurred, which was also previously observed for Fe$_2$(p-dobdc) and attributed to oxidation of Fe^{2+} to Fe^{3+} upon exposure to air, followed by decomposition of the MOF.[20,28] For better illustration, Fig. 1d shows the time evolution of the normalized intensity of the $\nu(C{=}C_{Ar})$ mode at 1410 cm^{-1} up to 180 s. The intensity passed through a maximum at *ca.* 12 s, followed by a decline that coincided with the formation of another product after 2000 s (Fig. 1c). After isolation, the XRD pattern of this reaction product indicated a lack of crystallinity (Fig. S2), confirming the absence of the MOF structure.

Although MOF decomposition occurred in this experiment, we were able to observe the rapid formation of a MOF product (likely Fe$_2$(p-dobdc)) in its early stages. The most probable reason for the failure of this synthesis is the presence of air and the known Fe-MOF air sensitivity. Therefore, the experimental setup was modified to include a supply of inert gas and an enclosure with the goal of keeping the whole reaction volume air-free (Fig. S3).

Once the degassed ligand solution was added to the inertized Fe(ClO$_4$)$_2$ solution inside the ATR-IR cell, the behavior of the system was markedly different compared to that obtained under air. The $\nu(C{=}C_{Ar})$ mode emerged rapidly and intensified steadily, confirming the formation of the MOF (Fig. 1d). The spectrum of the final product after 2000 s (Fig. 1c, offset) resembles closely the spectrum of the product obtained after 12 s in the synthesis conducted under air.

These findings indicate that the formation of MOF is possible under inert conditions within extended time periods that can allow the synthetic utility of this method. To further shed light on the process of MOF formation in these conditions, *in situ* synchrotron XRD was employed to prove that the MOF material is formed and to follow its crystallization more closely.

The aqueous phase synthesis of Zn-MOF-74[29] delivered purer materials when 2.5 eq. of a metal salt were used instead of the stoichiometric 2 eq., which also speeds up the reaction,
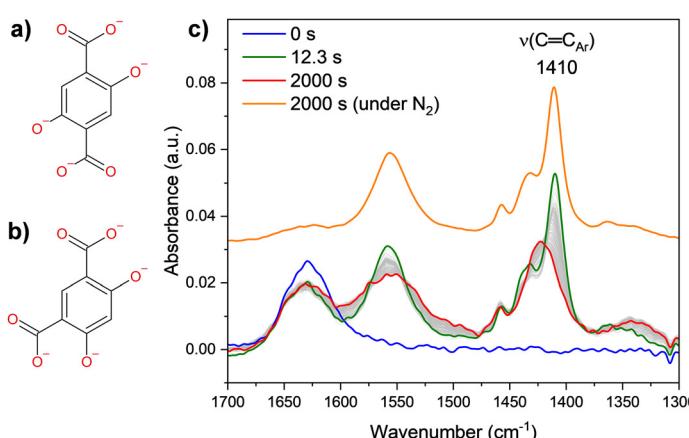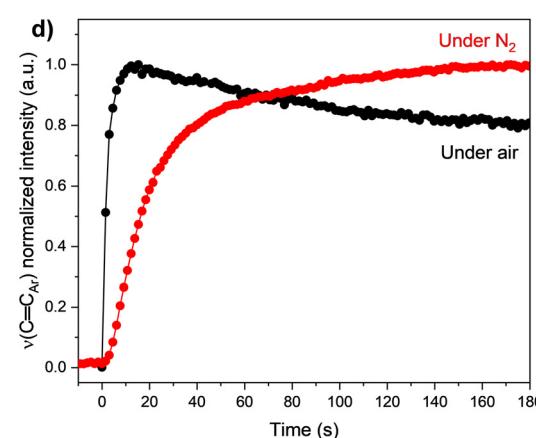

Fig. 1 Structures of (a) p-dobdc^{4-} and (b) m-dobdc^{4-} ligands. (c) Sequence of *in situ* ATR-IR spectra during synthesis of Fe$_2$(p-dobdc) under air and (offset) spectrum of the final product obtained during synthesis under N$_2$. (d) Normalized intensities of the $\nu(C{=}C_{Ar})$ mode at 1410 cm^{-1} for experiments under N$_2$ and under air.

ensuring a nearly full ligand consumption. Hence, during the measurements with high-energy X-rays, 2.5 eq. of the Fe salt were used to ensure a smoother reaction and to provide an excess of reducing agent in the reaction mixture, in case minute air amounts are present in the modified setup for synchrotron experiments. The raw XRD data were subjected to a multi-step treatment where key parameters of the $Fe_2(p\text{-}dobdc)$ phase were extracted, namely, lattice parameters, characteristic peak FWHM (linked to particle size), and degree of crystallinity (α, representing the amount of the MOF phase in the system).

Comparison of an XRD pattern obtained during *in situ* synthesis with the simulated one for this material (Fig. 2a) proved that the product was effectively $Fe_2(p\text{-}dobdc)$. The time evolution of the MOF signal, namely the degree of crystallinity, α, (Fig. 2c), indicates its rapid formation within the first seconds of the synthesis. This difference with the ATR-IR data is explained by the excess of Fe^{2+} used in these experiments, which shifts the reaction equilibrium towards the product and enables the fast formation of the target MOF. To the best of our knowledge, this is the first time the formation of a MOF-74 type structure of $Fe_2(p\text{-}dobdc)$ is observed not only in a non-solvothermal, aqueous, room-temperature condition but with sub-second time resolution, considering that most of the product was formed after less than 8 s of reaction time. Following the reaction at earlier stages was not possible due to the setup specifics. Notably, the lattice parameters (Fig. 2b) were already stable after 8 s, indicating that most of the transformations leading to the formation and growth of MOF particles occurred prior to that point in time.

Only a slight decrease in the FWHM of the XRD peaks of the MOF was observed over the subsequent 100 s (Fig. 2d), which is attributed to a slight particle size increase owing to Ostwald ripening.[29,30] However, this peak width remained relatively large at *ca.* 0.03° (instrumental contribution, <0.01°), indicating a likely small particle size and/or residual strain in the MOF particles caused by their fast formation and the impossibility to recrystallize into larger, better-quality crystallites at room temperature.

Based on the knowledge that increased temperature allows for a recrystallization mechanism and enables the growth of well-crystallized, faceted particles, as exemplified in the aqueous synthesis of $Zn_2(p\text{-}dobdc)$,[29] the synthesis of $Fe_2(p\text{-}dobdc)$ was conducted at 80 °C in the *in situ* XRD cell. A different behaviour with a three-step process was observed (Fig. S4a–c), where in the first step (I) from 4 to 6 s, the rapid formation of an already well-crystalline $Fe_2(p\text{-}dobdc)$ occurred, as evidenced by the low peak width values. During product formation, the lattice parameters of the material evolved significantly. In the second step (II) up to 14 s, the lattice evolution continued and peaked, while the intensity of the MOF peaks slightly decreased. This indicates that a part of the material redissolved, owing to its metastable state with non-equilibrium lattice parameters. Finally, in the third step (III) up to *ca.* 80 s, the lattice parameters stabilized, and the peak intensity reached a plateau, pointing to the completion of the synthesis process. FWHM of the 110 and 300 peaks (Fig. S4c) decreased steadily over these three steps, mirroring the continuous increase of the average particle size of the material, a behaviour that we associate with the continuing dissolution/recrystallization process.

The absolute values of unit cell volume of 4075 Å^3 (25 °C) and 4085 Å^3 (80 °C) of $Fe_2(p\text{-}dobdc)$ are comparable to the reported value of 4082 Å^3 for the fresh material containing Fe^{2+} rather than to 3905 Å^3, which characterized the material oxidized upon air-exposure and containing Fe^{3+}.[28] This provides structural evidence for the presence of Fe in oxidation state +2 in this sample. Following the success of the $Fe_2(p\text{-}dobdc)$ synthesis and
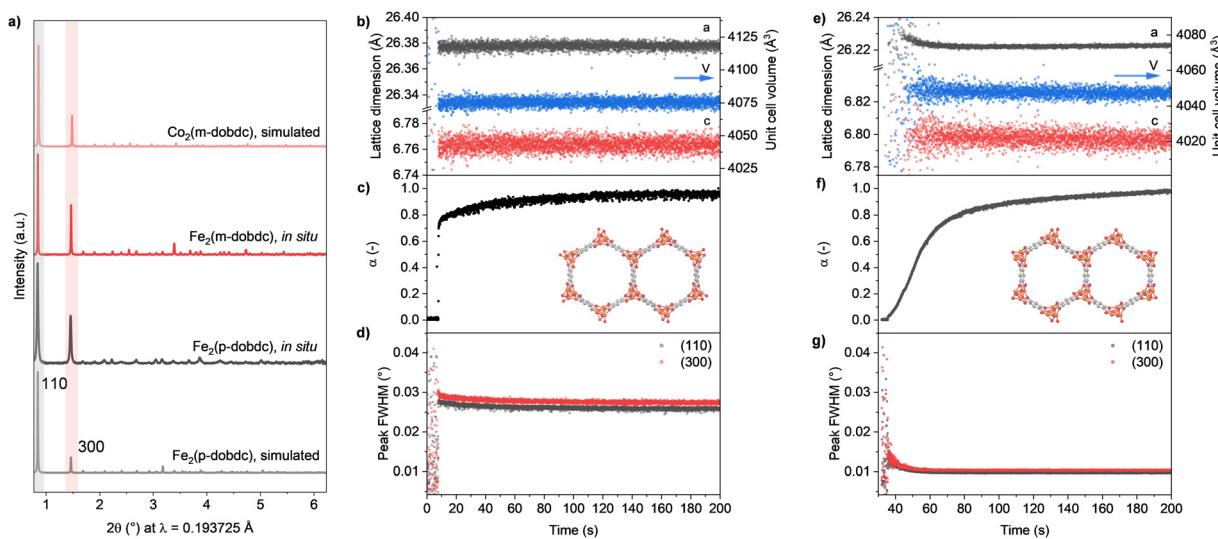

Fig. 2 (a) XRD patterns of $Fe_2(p\text{-}dobdc)$ and $Fe_2(m\text{-}dobdc)$ obtained at the end of synthesis in N_2 and corresponding simulated patterns. The region is magnified 7× for the simulated pattern of $Co_2(m\text{-}dobdc)$ and 3× for other patterns for the sake of visual clarity. Evolution of (b) lattice parameters, (c) degree of crystallinity (α), (d) FWHM of the 110 and 300 peaks during synthesis of $Fe_2(p\text{-}dobdc)$ in N_2 at 25 °C. Evolution of (e) lattice parameters, (f) degree of crystallinity (α), (g) FWHM of the 110 and 300 peaks during synthesis of $Fe_2(m\text{-}dobdc)$ in N_2 at 25 °C. Insets in (c) and (f) represent the crystal structures of $Fe_2(p\text{-}dobdc)$ and $Fe_2(m\text{-}dobdc)$, respectively. Atom colors: Fe, brown; O, red; C, gray; hydrogen atoms are omitted for clarity.
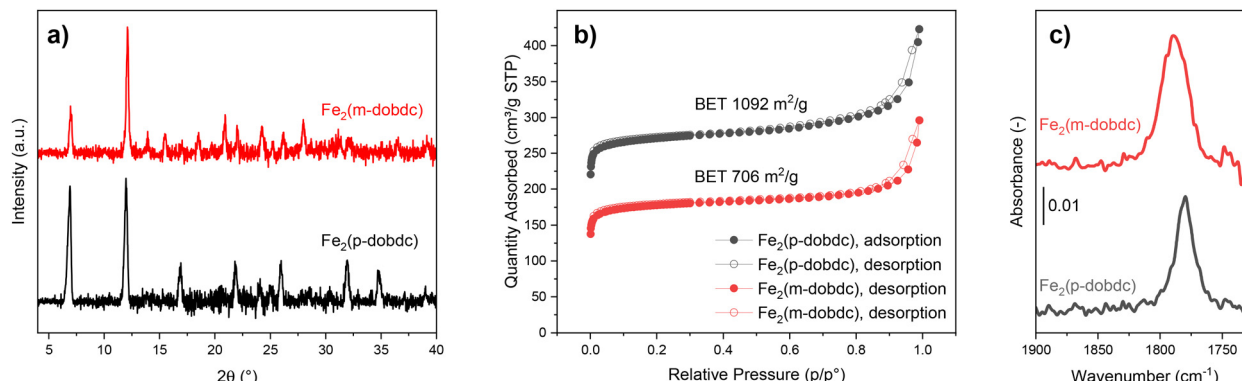
Fig. 3 (a) XRD patterns, (b) N_2 adsorption isotherms at 77 K of $Fe_2(p\text{-dobdc})$ and $Fe_2(m\text{-dobdc})$, and (c) *in situ* ATR-IR spectra after adsorption of NO at 25 °C.

showcasing the feasibility of aqueous Fe-based MOF synthesis, we attempted to widen the synthetic space by choosing 4,6-dihydroxy-1,3-isophthalic acid, $H_4(m\text{-dobdc})$, as a further linker. The corresponding material $Fe_2(m\text{-dobdc})$ is a structural isomer of $Fe_2(p\text{-dobdc})$ (insets of Fig. 2c and f) and, albeit featuring a more available and inexpensive linker, can be produced only using solvothermal methods.[31] *In situ* XRD showed that the process of the $Fe_2(m\text{-dobdc})$ formation was slower at 25 °C, while yielding a well-crystalline material with low FWHM values after *ca.* 120 s. This is notably slower than the synthesis of the para analogue, which can be explained by a more strained and distorted structure of $Fe_2(m\text{-dobdc})$ compared to $Fe_2(p\text{-dobdc})$, making the synthesis process more reversible and allowing the recrystallization and ripening take place to provide a well-crystallized material. The correspondence of the XRD pattern of $Fe_2(m\text{-dobdc})$ with the simulated structure (Fig. 2a) confirms the phase-pure nature of the product, thus revealing the practical feasibility of the aqueous phase synthesis method.

The practical feasibility of the aqueous phase synthesis method was further explored by producing the same materials in the laboratory using optimized conditions gathered from the *in situ* experiments and by isolating them for characterization. We shall note that although the activation procedure currently employs methanol, the synthetic step aligns with green chemistry principles such as safer solvent use and energy efficiency. Future studies may further optimize the work-up to achieve a fully solvent-minimized process.

Both MOFs were produced with high crystallinity (Fig. 3a) and typical values of specific surface area (Fig. 3b). The reduced data quality of in-house XRD is instrumental in origin rather than structural, as an inert sample holder and Fe fluorescence significantly decrease the signal-to-noise ratio. However, the diffraction pattern confirms that the bulk phase obtained under inert conditions at lab scale is consistent with that observed *in situ* by high-energy XRD. The intensity differences among the peaks are attributed to varying degrees of hydration between the sample obtained in the *in situ* XRD cell and the one produced in-house.

The oxidation state of Fe that could not be characterized directly during synthesis was identified by *in situ* NO adsorption. Fe^{2+} is known to selectively chemisorb NO, with the position of the $\nu(N\text{–}O)$ vibrational mode in IR spectra indicating the type of Fe–NO interaction. *In situ* ATR-IR spectra of the layers of the materials prepared in the glovebox and activated in Ar in the cell (Fig. 3c and Fig. S5) showed the emergence of peaks at 1779 cm^{-1} and 1789 cm^{-1} for $Fe_2(p\text{-dobdc})$ and $Fe_2(m\text{-dobdc})$, respectively. These values are significantly red-shifted compared to the vibrational frequency of pure NO (1876 cm^{-1}), in agreement with a strong charge transfer from Fe ions to NO. Previous observations of NO adsorbed on $Fe_2(p\text{-dobdc})$ reported $\nu(N\text{–}O)$ at 1782 cm^{-1} [32], thus confirming the Fe^{2+} oxidation state in the materials produced with the new aqueous method in an inert atmosphere. Although complementary spectroscopic analysis (*e.g.*, XPS, XANES) could further validate the oxidation state of Fe, the combined structural and spectroscopic evidence presented here strongly supports the presence of Fe^{2+} ions in the as-synthesized materials.

In summary, this work demonstrates the rapid and facile synthesis for Fe-based members of the MOF-74 series in water under ambient conditions. Guided by *in situ* ATR-IR spectroscopy and synchrotron XRD, we developed optimal synthetic conditions for two materials, $Fe_2(p\text{-dobdc})$ and $Fe_2(m\text{-dobdc})$, which were characterized for their structure and were confirmed to contain Fe in oxidation state +2, thus opening pathways for their scalable synthesis. This synthesis route is clearly advantageous compared to more demanding solvothermal methods. Further work could focus on obtaining deeper insights into the redox processes during the synthesis and workup of these materials.

Conflicts of interest

There are no conflicts to declare.

Data availability

Data for this article are available at Zenodo at **https://doi.org/10.5281/zenodo.15823570**.

Supplementary information (SI): details of experimental procedure such as synthesis and setups, ATR-IR spectra, XRD patterns and analysis of XRD patterns. See DOI: **https://doi.org/10.1039/d5ma00842e**.

Acknowledgements

Notes and references

1 (a) K. K. Gangu, S. Maddila, S. B. Mukkamala and S. B. Jonnalagadda, Inorg. Chim. Acta, 2016, **446**, 61–74; (b) H. C. Zhou, J. R. Long and O. M. Yaghi, Chem. Rev., 2012, **112**, 673–674.

2 (a) H. Furukawa, K. E. Cordova, M. O'Keeffe and O. M. Yaghi, Science, 2013, **341**, 1230444; (b) L. R. MacGillivray, Metal–organic frameworks: design and application, John Wiley & Sons, 2010.

3 M. Safaei, M. M. Foroughi, N. Ebrahimpoor, S. Jahani, A. Omidi and M. Khatami, Trends Anal. Chem., 2019, **118**, 401–425.

4 (a) A. J. Howarth, A. W. Peters, N. A. Vermeulen, T. C. Wang, J. T. Hupp and O. K. Farha, Chem. Mater., 2017, **29**, 26–39; (b) S. Yuan, L. Feng, K. Wang, J. Pang, M. Bosch, C. Lollar, Y. Sun, J. Qin, X. Yang and P. Zhang, Adv. Mater., 2018, **30**, 1704303.

5 P. A. Julien, C. Mottillo and T. Friščić, Green Chem., 2017, **19**, 2729–2747.

6 Y.-R. Lee, J. Kim and W.-S. Ahn, Korean J. Chem. Eng., 2013, **30**, 1667–1680.

7 W. L. Teo, W. Zhou, C. Qian and Y. Zhao, Mater. Today, 2021, **47**, 170–186.

8 N. Stock and S. Biswas, Chem. Rev., 2012, **112**, 933–969.

9 Y. Sun and H.-C. Zhou, Sci. Technol. Adv. Mater., 2015, **16**, 054202.

10 K. Hartonen and M.-L. Riekkola, The application of green solvents in separation processes, Elsevier, 2017, pp. 19–55.

11 L. Lajoie, A.-S. Fabiano-Tixier and F. Chemat, Pharmaceuticals, 2022, **15**, 1507.

12 (a) M. A. Artsiusheuski, N. P. M. Casati, A. H. Clark, M. Nachtegaal, R. Verel, J. A. van Bokhoven and V. L. Sushkevich, Angew. Chem., Int. Ed., 2025, **64**, e202415919; (b) X. Liu, X. Wang and F. Kapteijn, Chem. Rev., 2020, **120**, 8303–8377.

13 S. Kumar, S. Jain, M. Nehra, N. Dilbaghi, G. Marrazza and K.-H. Kim, Coord. Chem. Rev., 2020, **420**, 213407.

14 L. Huelsenbeck, H. Luo, P. Verma, J. Dane, R. Ho, E. Beyer, H. Hall, G. M. Geise and G. Giri, Cryst. Growth Des., 2020, **20**, 6787–6795.

15 (a) K. Guesh, C. A. D. Caiuby, Á. Mayoral, M. Díaz-García, I. Díaz and M. Sanchez-Sanchez, Cryst. Growth Des., 2017, **17**, 1806–1813; (b) J. Huo, M. Brightwell, S. ElHankari, A. Garai and D. Bradshaw, J. Mater. Chem. A, 2013, **1**, 15220–15223; (c) M. Sánchez-Sánchez, N. Getachew, K. Díaz, M. Díaz-García, Y. Chebude and I. Díaz, Green Chem., 2015, **17**, 1500–1509; (d) J. M. Yassin, A. M. Taddesse and M. Sánchez-Sánchez, Microporous Mesoporous Mater., 2021, **324**, 111303.

16 J. Fonseca, T. Gong, L. Jiao and H.-L. Jiang, J. Mater. Chem. A, 2021, **9**, 10562–10611.

17 (a) H. Deng, S. Grunder, K. E. Cordova, C. Valente, H. Furukawa, M. Hmadeh, F. Gandara, A. C. Whalley, Z. Liu, S. Asahina, H. Kazumori, M. O'Keeffe, O. Terasaki, J. F. Stoddart and O. M. Yaghi, Science, 2012, **336**, 1018–1023; (b) H. Kim and C. S. Hong, CrystEngComm, 2021, **23**, 1377–1387.

18 J. H. Choe, H. Kim and C. S. Hong, Mater. Chem. Front., 2021, **5**, 5172–5185.

19 (a) E. D. Bloch, W. L. Queen, R. Krishna, J. M. Zadrozny, C. M. Brown and J. R. Long, Science, 2012, **335**, 1606–1610; (b) P. Verma, X. Xu and D. G. Truhlar, J. Phys. Chem. C, 2013, **117**, 12648–12660.

20 E. D. Bloch, L. J. Murray, W. L. Queen, S. Chavan, S. N. Maximoff, J. P. Bigi, R. Krishna, V. K. Peterson, F. Grandjean, G. J. Long, B. Smit, S. Bordiga, C. M. Brown and J. R. Long, J. Am. Chem. Soc., 2011, **133**, 14814–14822.

21 L. J. Wang, H. Deng, H. Furukawa, F. Gándara, K. E. Cordova, D. Peri and O. M. Yaghi, Inorg. Chem., 2014, **53**, 5881–5883.

22 L. Garzón-Tovar, A. Carné-Sánchez, C. Carbonell, I. Imaz and D. Maspoch, J. Mater. Chem. A, 2015, **3**, 20819–20826.

23 J. Joseph, S. Iftekhar, V. Srivastava, Z. Fallah, E. N. Zare and M. Sillanpää, Chemosphere, 2021, **284**, 131171.

24 M. Pu, Y. Ma, J. Wan, Y. Wang, J. Wang and M. L. Brusseaud, Catal. Sci. Technol., 2017, **7**, 1129–1140.

25 Q. Huang, A. Zeb, Z. Xu, S. Sahar, J.-E. Zhou, X. Lin, Z. Wu, R. C. K. Reddy, X. Xiao and L. Hu, Coord. Chem. Rev., 2023, **494**, 215335.

26 (a) S. Kment, A. Bakandritsos, I. Tantis, H. Kmentová, Y. Zuo, O. Henrotte, A. Naldoni, M. Otyepka, R. S. Varma and R. Zbořil, Chem. Rev., 2024, **124**, 11767–11847; (b) C. H. Hendon, A. J. Rieth, M. D. Korzyński and M. Dincă, ACS Cent. Sci, 2017, **3**, 554–563.

27 F. J. Valverde-Muñoz, M. Seredyuk, M. C. Muñoz, K. Znovjyak, I. O. Fritsky and J. A. Real, Inorg. Chem., 2016, **55**, 10654–10665.

28 M. Märcz, R. E. Johnsen, P. D. C. Dietzel and H. Fjellvåg, Microporous Mesoporous Mater., 2012, **157**, 62–74.

29 I. Kochetygov, L. Maggiulli, M. Ranocchiari and D. Ferri, Chem. Mater., 2024, **36**, 6877–6887.

30 B. L. Bonnett, S. Ilic, K. Flint, M. Cai, X. Yang, H. D. Cornell, A. Taylor and A. J. Morris, Inorg. Chem., 2021, **60**, 10439–10450.

31 M. T. Kapelewski, S. J. Geier, M. R. Hudson, D. Stück, J. A. Mason, J. N. Nelson, D. J. Xiao, Z. Hulvey, E. Gilmour, S. A. Fitzgerald, M. Head-Gordon, C. M. Brown and J. R. Long, J. Am. Chem. Soc., 2014, **136**, 12119–12129.

32 E. D. Bloch, W. L. Queen, S. Chavan, P. S. Wheatley, J. M. Zadrozny, R. Morris, C. M. Brown, C. Lamberti, S. Bordiga and J. R. Long, J. Am. Chem. Soc., 2015, **137**, 3466–3469.